

## DEFORMATION MONITORING USING REMOTELY SENSED RADAR INTERFEROMETRIC DATA

Michele Crosetto<sup>1</sup>, Alain Arnaud<sup>2</sup>, Javier Duro<sup>2</sup>, Erlinda Biescas<sup>1</sup> and Marta Agudo<sup>1</sup>

<sup>1</sup> *Institute of Geomatics, Campus de Castelldefels, Avinguda del Canal Olímpic s/n,  
E-08860 Castelldefels (Barcelona), Spain*

<sup>2</sup> *Altamira Information SL, Carrer Roger de Lúria, 50, àtic B, E-08009 Barcelona, Spain*

### Abstract

The paper focuses on the capabilities of SAR (Synthetic Aperture Radar) interferometry for the monitoring of deformations of the Earth surface. The paper begins with a concise description of different interferometric procedures, like the coherence-based techniques and the amplitude-based techniques. A brief discussion of some important aspects, like the flexibility of the interferometric techniques and their capability to support a fully quantitative monitoring of deformations is included. The conditions to achieve high quality standards with SAR interferometry are described. In particular, the techniques based on single image pairs and those based on multiple SAR images are compared. The last part of the paper illustrates the preliminary results obtained over the city of Barcelona (Spain) using a stack of 20 ERS SAR images and a coherence based technique.

### 1. Introduction

This paper describes the deformation monitoring of the Earth surface based on remotely sensed SAR (Synthetic Aperture Radar) data. The interferometric SAR techniques (InSAR) use the information contained in the phase of two SAR images. The InSAR phase is sensitive to the terrain topography and to relative changes in elevation occurring between two SAR antenna passes over the same area. If the terrain topography is known, i.e. a DEM (Digital Elevation Model) of the imaged scene is available, the corresponding phase component can be subtracted from the InSAR phase, leaving the component due to the terrain surface deformation. This is the so-called differential InSAR technique (DInSAR).

Since the first description of the technique (Gabriel et al., 1989), many DInSAR applications have been developed. The most important results have been obtained in different branch of geophysics: ice and glacier dynamics (Goldstein et al., 1993; Kwok and Fahnestock, 1996); earthquakes (Massonnet et al., 1993; Massonnet et al., 1994); volcanoes (Massonnet et al., 1995; Amelung et al., 2000); and landslides (Carnec et al., 1996). For a general review, see Hanssen (2001). Besides the geophysical applications, many studies have been conducted in urban areas, see for instance Amelung et al. (1999); Tesauro et al. (2000); Ferretti et al. (2000); Strozzi et al. (2001); Crosetto et al. (2002); and Crosetto et al. (2003).

DInSAR offers the typical advantages of the remote sensing techniques: it provides data over inaccessible areas and large area coverage (for instance, a scene of the ERS-2, one of the two operational SAR sensors of the European Space Agency, covers 100 by 100 km). Furthermore, it can (potentially) provide deformation measurements with a quality that is comparable with that of the traditional geodetic techniques. This point is discussed in detail below. However, it is important to underline that high quality results can only be achieved by employing an adequate InSAR processing (image registration, filtering, phase unwrapping, etc.), coupled with an appropriate statistical treatment of the DInSAR observations. Another important advantage of

the DInSAR technique is the availability of large time series of SAR images, which in the case of the ERS satellites cover more than a decade, starting from 1991. If a new deformation phenomenon is discovered (say, a subsidence in a suburban area, where new construction licenses have to be released), by DInSAR it is now possible to study the evolution of the given area in the last 10 years. This represents an unmatched capability compared with the traditional geodetic techniques, which for all phenomena characterized by low deformation rates require long observation periods.

The use of the D-InSAR technique is however affected by some important limitations, like the temporal decorrelation and the effects caused by different atmospheric conditions (atmospheric effects). Furthermore, some of the DInSAR limitations are related to the temporal evolution, the extension and the magnitude of the considered deformations. The slow deformation phenomena (let's say, few millimetres per year) are only detectable over large time intervals, where the SAR images usually have very low coherence. An exception occurs in the urban areas that can remain coherent even over years. The SAR resolution represents a second limitation. Using a typical 5-look azimuth compression, the ERS SAR images are characterised by a pixel footprint of about 20 by 20 m. Since an adequate sampling of a given deformation field has to be guaranteed, a limit on the minimum size of the detectable deformations is posed. The interferometric phase noise represents a further limitation, which is critical for all applications characterized by small deformation magnitudes.

This paper begins with a concise description of different D-InSAR procedures. This is followed by a discussion of the quality aspects of the DInSAR results. This section describes the two typical DInSAR scenarios: the DInSAR based on a single image pair, and the use of multiple interferograms. The last part of the paper illustrates the results obtained over the Barcelona area using a stack of 20 ERS SAR images.

## **2. DInSAR techniques**

In the last years different types of techniques have been developed and the capabilities of DInSAR have improved considerably. The DInSAR techniques can be classified as follows:

- A) Coherence based DInSAR with a single image pair;
- B) Coherence based DInSAR with multiple images;
- C) DInSAR based on Interest Points (IP) selected on multiple images.

The three main aspects that differentiate the above techniques are briefly discussed below.

The first one is the quality criterion adopted in the selection of the suitable pixels. As mentioned above, the loss of coherence results in a noisy interferometric phase. During the interferometric process it is possible to estimate the coherence (i.e. the correlation) of each interferogram pixel. The first two types of techniques (A and B) use this information for the pixel selection. The last class of techniques (C), which is based on stacks of images, uses as a criterion for pixel selection the stability of the SAR amplitude (Ferretti et al. 2000). The points selected with such a criterion are usually referred to as Permanent Scatterers (PS). In this context we prefer the more general term IP, because the PS technique is one specific patent pending procedure, which includes both the point selection and the estimation of the terrain deformation, the atmospheric contribution, etc.

The second aspect is the number of required SAR images. The first class of techniques (A) represents the traditional DInSAR approach, which only requires a couple of images. The other two classes of techniques use time series of co-registered images, i.e. require much more data (data redundancy). As it is discussed in the following section, this aspect represents the key factor to achieve deformation-monitoring performances that are comparable to those of the geodetic techniques.

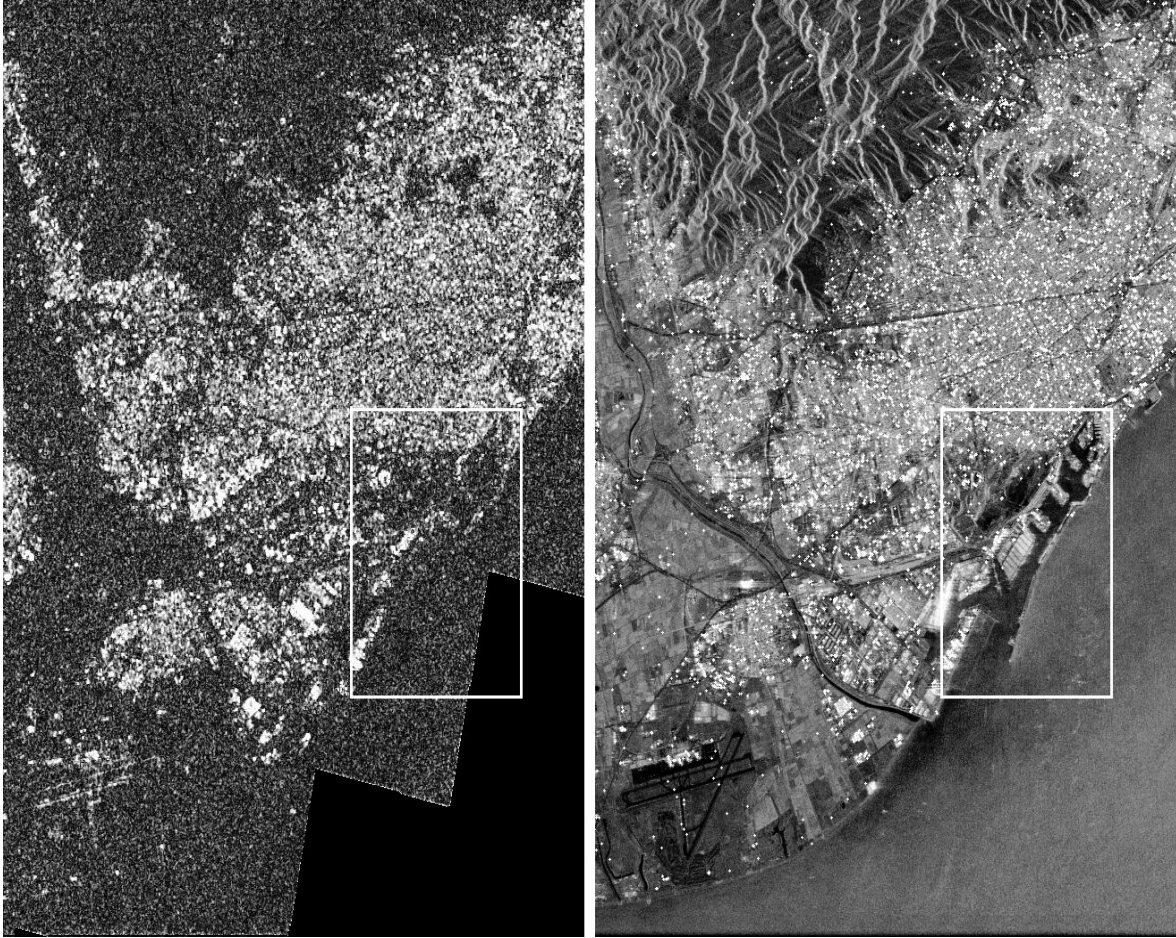


Fig. 1: Data availability for deformation control using two different DInSAR techniques over the Barcelona area. Coherence of an ERS-2 interferogram with a perpendicular baseline of 108 m and time interval of 1540 days (left side). The image has 132600 pixels with coherence above 0.5. On the right side, distribution of the IPs estimated with a stack of 20 images. The IPs are superposed to the mean amplitude of the 20 SAR images. One may recognize the centre of Barcelona, the Llobregat River, the port and the airport. There are 5956 IPs with  $D_A < 0.25$ , see Ferretti et al. (2001). The white frame indicates the area reported in Fig. 2.

The last aspect is the type of employed phase unwrapping procedure (i.e. the estimation of the phase ambiguities), see Ghiglia and Pritt (1998). The techniques of the classes A and B include in their procedure a traditional phase unwrapping algorithm, while some of the IP based techniques may avoid this step by resolving the phase ambiguity during the estimation of the deformations, see Ferretti et al. (2001). A key factor for the flexibility of the coherence based techniques (A and B) is the type of employed phase unwrapping. In fact, a strong limitation of most of the unwrapping algorithms is that they only work properly over long-term coherent areas, like the urban areas. Beside these areas, the SAR images often contain isolated targets that remain coherent over very large time periods. The traditional unwrapping techniques, which work on regular grids of SAR data, are incapable to unwrap these isolated targets. On the other hand, using suitable techniques that work on sparse sets of SAR data, it is possible to exploit the interferometric phase over these targets. The results discussed in this paper were obtained with a phase unwrapping for sparse data, which implements an algorithm similar to that described in Costantini and Rosen (1999).



Fig. 2: Data availability for deformation control using two different DInSAR techniques: zoom on the framed area from Fig. 1. Coherence image (left side) and IPs estimated with a stack of 20 images superposed to the mean amplitude of the 20 SAR images. In order to ease the comparison, the coherence image was manually masked. There are 8916 pixels with coherence above 0.5, while only 422 IPs with  $D_A$  below 0.25.

The flexibility of the different DInSAR procedures represents a fundamental factor for their applicability. The IP based techniques only exploit the targets that are stable over a time series of SAR images. This criterion is quite selective. On one hand it allows the best quality standards to be achieved, while on the other hand it gives little flexibility to the technique. In fact, outside the urban areas it is quite common to have a very low density of IPs, which is often inadequate for the sampling of small-scale deformation phenomena. This clearly represents an important limiting factor of these techniques. The same may occur in urban areas. Let us illustrate this limitation by analysing an example over the city of Barcelona (Spain). In Fig. 1 (left side) is illustrated the coherence of an interferogram with a time interval of 1540 days: there are 132600 pixels of good quality (coherence above 0.5). On the right side are illustrated the IPs estimated with a stack of 20 images: there are only 5956 IPs, which can be considered suitable for the IP based techniques (amplitude dispersion index  $D_A$  less than 0.25, see Ferretti et al. (2000)). This important difference in the available pixel density can definitely “make the difference” in the capability of DInSAR to support certain types of applications. To illustrate this, let us zoom on a small portion of Barcelona, assuming that an important infrastructure like the port requires a monitoring of its deformation (see Fig. 2). In this area there are 8916 pixels with coherence above 0.5, while there are only 422 IPs with  $D_A$  below 0.25. This means that only the coherence-based techniques could be used to monitor this area, while the available density of IPs is clearly not sufficient to perform the same task.

### 3. Quantitative deformation monitoring

This section briefly discusses the DInSAR capability to support a fully quantitative monitoring of deformations. Although a qualitative use of the DInSAR results seems to be sufficient for the purposes of some geophysical applications, this is not the case for some other important applications, e.g. the deformation control in urban areas, which need to be characterised by high quality standards like those usually achieved by the geodetic techniques. In geodesy, three important quality aspects are typically considered: the precision, accuracy and reliability of the estimates. It is evident that for the DInSAR technique, which is claimed to provide “geodetic quality”, the same aspects have to be considered. This is usually not the case, since in the literature there is even some confusion associated with the use of the above-mentioned terms.

The key factor to achieve a quantitative DInSAR deformation monitoring is the number of available interferograms (i.e. observations). The classical DInSAR configuration is based on a single interferogram, derived from a pair of complex SAR images. This is the simplest DInSAR configuration, which often is the only one that can be implemented, due to the limited data availability: the results of most DInSAR applications are derived using a single interferometric pair. This is a zero redundancy configuration. With such a configuration it is not possible to check the presence of the different errors that may affect the interferometric observations: the deformation estimates are not reliable. Note that the same occurs for the digital elevation models derived with single InSAR pairs.

The errors associated with the DInSAR observations have different origins. Among the most important we can include the unwrapping-related errors, the residual topographic component due to DEM errors, and the atmospheric artefacts. The unwrapping-related errors usually occur in low coherence areas, where the interferometric phase noise is high. In order to avoid these areas, the phase unwrapping for sparse data can be used. However, if the coherence is too low the density of the good pixels can be not sufficient to guarantee a correct sampling of the deformation signal. The residual topographic component can represent an important error source if large baselines are used and the quality of the DEM is not known. Finally, the atmospheric artefacts represent a very important error source, which can strongly degrade the quality of the DInSAR observations. All these error sources represent a strong limitation of the DInSAR technique based on a single interferogram. It is however important to underline that the usefulness of this simple configuration is context dependent. For instance, in all applications with strong deformations (e.g. co-seismic displacements of the order of meters) the magnitude of the above mentioned errors surely would not hide the deformation signal. Furthermore, the availability of a priori information on the phenomenon under analysis may reduce the impact of these errors. For instance, dealing with small-scale subsidences, where the location of the stable areas around the subsidence is known is it possible to reduce the influence of the atmospheric artefacts, see the least squares (LS) collocation procedure of Crosetto et al. (2002). On the other hand, these errors cannot be fully controlled and the deformation estimates cannot support a quantitative monitoring of the deformations.

A fully quantitative DInSAR monitoring may only be achieved by using multiple interferograms, i.e. multiple observations of the phenomenon under analysis. However, this is just a necessary condition, which is not sufficient to yield high quality DInSAR results. Two other conditions have to be fulfilled. Firstly, a very careful DInSAR processing has to be implemented. The quality of all major processing steps (e.g. image focussing, image registration, interferogram filtering, phase unwrapping, etc.) must be controlled through automatic or semi-automatic procedures. Note that the control of some steps, like the phase unwrapping may be time consuming. Secondly, suitable data modelling and analysis procedures have to be employed. In particular, an appropriate statistical treatment of the DInSAR observations is required. This fundamental step has been often disregarded.

A detailed description of a data modelling and analysis procedure for DInSAR data is beyond the scope of this paper. We briefly recall some basic properties of the DInSAR observations.

The D-InSAR phase  $\Delta\Phi_{D-Int}$  consists of the following components:

$$\Delta\Phi_{D-Int} = \Delta\Phi_{Int} - \Phi_{Topo\_Sim} = \Phi_{Mov} + \Phi_{Atm} + \Phi_{Res\_Topo} + \Phi_{Noise}$$

where  $\Delta\Phi_{Int}$  is the InSAR phase;  $\Phi_{Topo\_Sim}$  is the topographic phase component, simulated using a DEM;  $\Phi_{Mov}$  is the terrain deformation component;  $\Phi_{Atm}$  is the atmospheric contribution;  $\Phi_{Res\_Topo}$  represents the residual component due to DEM errors; and  $\Phi_{Noise}$  is the phase noise. When multiple DInSAR observations are available, the following properties may be exploited.  $\Phi_{Mov}$  is usually correlated, spatially and temporally, while  $\Phi_{Atm}$  is correlated spatially, and uncorrelated temporally. For a given pixel  $\Phi_{Res\_Topo}$  is a function of the DEM error and of the normal baseline of each interferogram. Finally,  $\Phi_{Noise}$  is spatially and temporally uncorrelated.

In order to exploit the above properties, 3D (2D in space plus the time) modelling and data analysis tools are required. In the literature these procedures have received little attention. Few authors have proposed pixel wise procedures that connect the observations of a single pixel with a one-dimensional model, see Berardino et al. (2001) and Ferretti et al. (2000). Strozzi et al. (2001) simply compute the average of multiple interferograms (interferogram stacking). The authors have implemented a new model, which allows the deformation velocity, the DEM error and the atmospheric component of each interferogram to be estimated by LS adjustment. The procedure provides the estimates with their associated standard deviations and supports the classical Baarda data snooping (Baarda, 1968). The preliminary results obtained with this procedure are summarized below.

#### 4. Results

This section briefly discusses the first results obtained over the Barcelona test side, which includes a quite stable area. 20 ERS-1 and ERS-2 SAR images were chosen as a training set for the implementation of the above-mentioned DInSAR model. The images span a time interval of about 5 years, from June 1995 to August 2000. The original SAR RAW data were processed with the software DIAPASON version 4.0, developed at the France National Space Centre (CNES) and distributes by Altamira Information, see <http://www.altamira-information>. From the SLC images, 20 interferograms were computed, see Table 1.

Int. #	B <sub>L</sub> [m]	ΔT [days]	Master Date	Slave Date	Int. #	B <sub>L</sub> [m]	ΔT [days]	Master Date	Slave Date
Int1	-5.6	665	19970830	19990626	Int14	60.3	945	19970621	20000122
Int3	17.7	665	19950617	19970412	Int16	81.1	839	19970412	19990730
Int4	-31.2	350	19951104	19961019	Int18	-82.7	805	19950617	19970830
Int5	27.4	1085	19970412	20000401	Int19	-88.3	1470	19950617	19990626
Int6	-38.4	210	19990626	20000122	Int20	-100.0	1401	19951103	19990904
Int7	-43.9	875	19970830	20000122	Int21	98.6	735	19970621	19990626
Int9	48.2	595	19951104	19970621	Int22	98.8	1504	19950617	19990730
Int10	-53.7	246	19990730	20000401	Int26	-108.2	385	19970621	19980711
Int11	88.2	1750	19950617	20000401	Int28	108.5	1540	19951104	20000122
Int13	-60.1	980	19951104	19980711	Int29	-106.0	805	19970412	19990626

Table 1: Characteristics of the 20 interferograms used in the Barcelona test side.

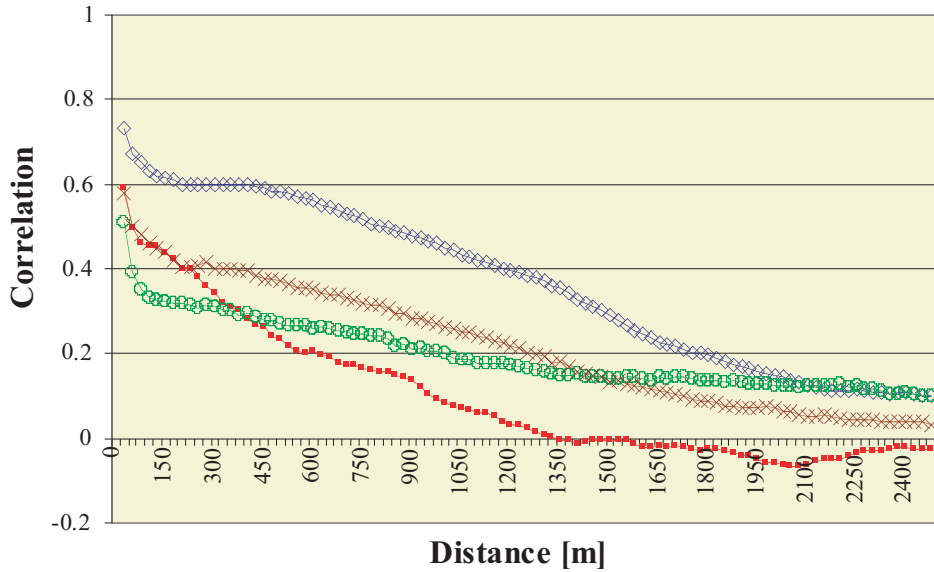


Figure 3: LS adjustment: autocovariance functions of the residuals of four interferograms.

The temporal baselines ( $\Delta T$ ) span from 246 to 1750 days, while the normal baselines ( $B_{\perp}$ ) are distributed in the range from  $-108$  to  $108$  m. For the data analysis we used sub-images of  $1100$  by  $1100$  pixels. Since the images were compressed in azimuth 5 times, they cover approximately  $22$  by  $22$  km. The coherence of all the processed interferograms is high, see the coherence of Int28 in Fig. 1, i.e. in the entire Barcelona urban and sub-urban area there is a good density of coherent pixels. We adopted a coherence-based procedure. For the phase unwrapping, a coherence threshold of  $0.5$  was used, i.e. a sparse grid of points was chosen on each interferogram. The unwrapped phases (with their associated standard deviations, derived from the coherence) were used as input of LS adjustment, in order to derive the estimation of the deformation velocity field and the DEM error. An important feature of the procedure is the capability to include in the adjustment observations coming from external sources. In this case we exploited the a priori available information concerning stable areas in the Barcelona downtown. In other cases, it would be useful to include in the adjustment observations coming from other data sources, like geodetic levelling campaign, GPS observations, etc.

We obtained so far only preliminary results. In general, in the considered area there is no significant deformation. However, there are three small portions of the city, which seem to be interested by some deformation phenomena. In the short future we will analyse more in depth these results. An important step will be the analysis of the quality of the adopted model, which makes two main assumptions: a constant velocity for each pixel and a linear trend, due to the atmospheric effects, for each interferogram. A useful tool in the model evaluation is the analysis of the residuals of each interferogram after the LS adjustment. Ideally, the residuals should be spatially uncorrelated (white noise). This is not the case with the results obtained so far, see in Fig. 3 the high spatial correlation of the residual of four interferograms over Barcelona. This correlation indicates that a further refinement of the adopted model is required.

### Acknowledgements

The authors thank Prof. Bruno Crippa from the Department of Geophysics of the University of Milan, for his advice and support in the data analysis of the DInSAR Barcelona test side.

## References

- Amelung, F., D.L. Galloway, J.W. Bell, H.A. Zebker and R.J. Lacznik (1999). Sensing the ups and downs of Las Vegas: InSAR reveals structural control of land subsidence and aquifer-system deformation. *Geology*, 27(6), 483-486.
- Amelung, F., S. Jonson, H.A. Zebker and P. Segall (2000). Widespread uplift and 'trapdoor' faulting on Galapagos volcanoes observed with radar interferometry. *Nature*, 407, 993-996.
- Baarda, W. (1968). A testing procedure for use in geodetic networks. Netherlands Geodetic Commission – *Publications on Geodesy*, Vol. 2, No. 5, Delft (Holland).
- Berardino, P., G. Fornaro G., A. Fusco A., et al. (2001). A new approach for analysing the temporal evolution of earth surface deformations based on the combination of DIFSAR interferograms. Proceedings of IGARSS 2001, Sidney (Australia), in CD.
- Carnec, C., D. Massonnet and C. King (1996). Two examples of the use of SAR interferometry on displacement fields of small spatial extent. *Geophys. Research Letters*, 23(24), 3579-3582.
- Costantini, M. and P. Rosen (1999). A generalized phase unwrapping approach for sparse data. *Proc. Int. Geosci. Remote Sensing Symp.*, Hamburg, Germany, June 28-July 2 1999, pp. 267-269.
- Crosetto, M., C.C. Tschering, B. Crippa and M. Castillo (2002). Subsidence Monitoring using SAR interferometry: reduction of the atmospheric effects using stochastic filtering. *Geophys. Research Letters*, Vol. 29(9), 26-29.
- Crosetto, M., M. Castillo and R. Arbiol (2003). Urban subsidence monitoring using radar interferometry: Algorithms and validation. *Photogrammetric engineering and remote sensing*, in press.
- Ferretti, A., C. Prati and F. Rocca (2000). Nonlinear subsidence rate estimation using the Permanent Scatterers in differential SAR interferometry. *IEEE Transactions on Geoscience and Remote Sensing*, 38(5), 2202-2012.
- Ferretti, A., C. Prati and F. Rocca (2001). Permanent scatterers in SAR interferometry. *IEEE Transactions on Geoscience and Remote Sensing*, 39(1), 8-20.
- Gabriel, A.K., R.M. Goldstein and H.A. Zebker (1989). Mapping small elevation changes over large areas: differential radar interferometry. *J. of Geophys. Research*, 94(B7), 9183-9191.
- Ghiglia, D.C. and M.D. Pritt (1998). *Two-dimensional phase unwrapping: theory, algorithms and software*. John Wiley and Sons, New York, 493p.
- Goldstein, R.M., H. Englehardt, B. Kamb and R.M. Frolich (1993). Satellite radar interferometry for monitoring ice sheet motion: application to an Antarctic ice stream. *Science*, 262, 1525-1530.
- Kwok, R. and M.A. Fahnestock (1996). Ice sheet motion and topography from radar interferometry. *IEEE Transactions on Geoscience and Remote Sensing*, 34(1), 189-200.
- Hanssen, R. (2001). *Radar interferometry*. Kluwer Academic Publishers, Dordrecht, Holland, 308p.
- Massonnet, D., M. Rossi, C. Carmona, F. Adragna, G. Peltzer, K. Feigl and T. Rabaute (1993). The displacement field of the Landers earthquake mapped by radar interferometry. *Nature*, 364, 138-142.
- Massonnet, D., K. Feigl, M. Rossi and F. Adragna (1994). Radar interferometry mapping of deformation in the year after the Landers earthquake. *Nature*, 369, 227-230.
- Massonnet, D., P. Briole and A. Arnaud (1995). Deflation of Mount Etna monitored by spaceborne radar interferometry. *Nature*, 375, 567-570.
- Strozzi, T., U. Wegmuller, L. Tosi, G. Bitelli and V. Spreckels (2001). Land subsidence monitoring with differential SAR interferometry. *Photogrammetric engineering and remote sensing*, 67(11), 1261-1270.
- Tesauro, M., P. Berardino, R. Lanari, E. Sansosti, G. Fornaro and G. Franceschetti (2000). Urban subsidence inside the city of Napoli (Italy) observed by satellite radar interferometry. *Geophys. Research Letters*, 27(13), 1961-1964.